J. Fluid Mech. (1997), *vol.* 347, *pp.* 13–36 Printed in the United Kingdom

Solidifying Bingham extrusions: a model for the growth of silicic lava domes

By ROSS W. GRIFFITHS[1] AND JONATHAN H. FINK[2]

[1] Research School of Earth Sciences, the Australian National University, Canberra 0200 ACT, Australia

[2] Geology Department, Arizona State University, Tempe, AZ 85287-1404, USA

(Received 17 April 1996 and in revised form 16 April 1997)

In a previous study of the effects of cooling and solidification on flows issuing onto a horizontal plane and spreading under gravity we considered the case of a viscous fluid that solidifies to form a thin surface crust with a finite yield strength. In that case, the coupling of solidification and viscous stresses in the flow led to a sequence of flow regimes or styles of flow and crustal deformation. Here, we study the spreading, from a small source, of a plastic material having a yield strength before cooling. In this case the fluid again begins to freeze as it spreads radially under gravity, and forms a dome having a surface crust which is stronger than the extruded fluid. If cooling is sufficiently rapid compared to gravity-driven spreading, the flow is found to be controlled by solidification. The flow again takes on one of a number of flow regimes depending on the pace of solidification relative to the rate of lateral flow, or extrusion rate. However, these flow regimes are quite different from those for the viscous extrusions, implying that the internal yield stress has a strong influence on the behaviour. Styles of flow ranged from inflation of an axisymmetric dome to irregular extrusion of lateral lobes and vertical spines. These qualitatively different regimes have much in common with the eruption styles of volcanic lava domes produced by effusion of extremely viscous silicic magmas which may possess a yield strength, and the model provides information about the factors influencing the morphology and hazards of such volcanic flows.

1. Introduction

The flow of viscous lavas involves the effusion of magma from a vent and its spreading under gravity across a surface while cooling and solidifying. Insights into the dynamics of lava flows of the lowest viscosities ($\sim 10^3$–10^6 Pa s^{-1}) have been provided by theoretical and experimental studies of an interesting but complex fluid flow: the gravitational spreading at small Reynolds numbers and large Péclet numbers of a relatively simple viscous fluid while it is cooling from its free surface (Hallworth, Huppert & Sparks 1987; Fink & Griffiths 1990, 1992; Griffiths & Fink 1993). These studies were based on laboratory models and made use of a molten wax. The wax was injected beneath cold water in order to increase the cooling rates to values that gave significant solidification on the laboratory time scale (and which also scale appropriately to realistic lava cooling rates). The morphology, or structural features, of such solidifying flows is related to the rates of solidification and effusion. The flow behaviour for a given base topography is largely determined by a single dimensionless parameter, Ψ, defined as the ratio of a time scale for the onset of solidification at the

free surface of the flow as the fluid moves away from the source to a time scale for lateral viscous spreading that would apply in the absence of cooling. A sequence of four dominant flow regimes or morphologies was identified (Fink & Griffiths 1990, 1992). At the smallest values of Ψ the wax solidified rapidly and produced a pile of small bulbous 'pillows'. At increasing values of Ψ (slower solidification or more rapid flow) the extrusion formed large solid plates of thick crust which 'rifted' apart, or a thinner crust which was strongly deformed by transverse folds. At large values of Ψ, smaller amounts of solid formed as 'levees' around the flow front and inhibited advance of the flow at its margins.

With the assistance of scaling analyses (Griffiths & Fink 1993), conditions were also determined under which the flow was controlled by either the viscous stress acting over the basal area of the flow or the strength of the solid surface layer near the flow front. These ideas have been compared with the few terrestrial lava flows for which estimates of both lava viscosity and flow rates are available (Griffiths & Fink 1992*a*). Although these lavas cool predominantly by radiation (rather than by convection as in the experiments) the role of the parameter Ψ is not expected to be dependent on the heat transfer mechanism. Morphological features identified in the lavas are similar to those in the analogue experiments, and the values of Ψ for each morphology are consistent. Several different styles of flow are also observed in submarine lavas, and these too have been related to those in the laboratory analogue (Griffiths & Fink 1992*b*; Gregg & Fink 1995).

A primary aim of the modelling of solidifying viscous gravity currents has been to relate the morphology of lava flows to the dynamics of their emplacement. An apparent, or bulk, viscosity (Pinkerton 1987; Stasiuk, Jaupart & Sparks 1993) has often been introduced by volcanologists as a convenient method of describing the advance of mafic (low to medium viscosity) lava flow fronts in terms of a single averaged value of the mechanical properties of the material, but without describing the temperature and rheological variations within the flow. In this approach it is recognized that larger apparent viscosities can be a result of a larger magma viscosity at the vent, a greater magma yield strength resulting from large volume fractions of crystals or bubbles, or a greater rheological change due to cooling as the flow front advances. However, the concept of an apparent viscosity is of limited usefulness because progressive cooling and solidification will produce a time-dependent apparent viscosity, which cannot be simply related to the rheology of the erupted magma, nor to heat loss from the flow. The concept embodies little understanding of the dynamics of the flow.

In an earlier paper (Griffiths & Fink 1993) we showed that a very large apparent viscosity estimated for a dome of highly silicic and extremely 'stiff' (andesite) lava that grew in La Soufriere volcano on the island of St Vincent in 1979 (Huppert *et al.* 1982) can be replaced by the yield strength of a strong outer crust. Support of the dome by a crust yield strength is more consistent with the data for the growth of the dome volume, height and radius. Confinement of the stresses to a thin surface boundary layer is also consistent with the dome growth rate, which is large when compared with the rate of conduction of heat through the depth of the dome. We also compared the results of the scaling analyses of cooling flows with data for a lava dome in Mt St Helens (1980–86), formed by another extrusion of highly silicic and extremely viscous (dacite) lava, and again concluded that purely viscous models are unsatisfactory. The qualitative style of eruption, and the height measurements for the dome, are instead consistent with models in which growth was controlled by either an internal magma yield strength (as suggested by Blake 1990) or the strength of a strong outer crust (as

suggested by Iverson 1990). We conclude that in order to make progress it is necessary to go beyond the concept of an apparent viscosity for these complex flows and to take account of both the thermodynamics of the flow and non-viscous rheologies, at least in a cooling surface layer.

The importance of non-viscous rheologies will be obvious for most solidifying liquid flows and for flow of plastic materials. It is especially highlighted by the case of lavas having relatively large silica contents and therefore extremely large viscosities (andesite, dacite and rhyolite lavas having viscosities greater than 10^7 Pa s^{-1}). These are produced by eruption of magmas which, even before cooling, are extremely viscous and may also have a finite shearing strength at zero strain rate. A yield strength could result from large crystal contents (McBirney & Murase 1984; Kerr & Lister 1991), which are often above 50 % by volume in these magmas, and possibly from a large population of gas bubbles produced by exsolution of volatiles on reduction of pressure as the magma ascends through the volcanic plumbing system. For such large viscosities and with the possibility of a yield strength cooling can again be expected to produce a rheologically distinct outer crust, but the contrasts within the lava may be smaller than in less viscous lavas. An interior yield strength may also inhibit transport beneath the surface crust (the carapace) from the vent to distal regions of the flow.

An example is the dacite lava dome that grew on the summit of Mount Unzen in 1991–5 and which caused much damage through gravitational collapses of the flow front and generation of a number of pyroclastic flows (turbulent suspensions of very hot magma fragments and gas capable of travelling hundreds of kilometres per hour). This eruption formed a sequence of large lobes, with each enlarging until the continuing flow from the vent was diverted to begin forming a new lobe. For these highly silicic lavas it is not clear what roles cooling and yield strength play in the overall dynamics of the flow, or whether both influence the morphology. In particular, we do not know the conditions which determine whether the style of dome growth is by inflation ('endogenous'), by extrusion of multiple lobes ('exogenous'), or by a combination of these processes (Fink, Malin & Anderson 1990). The behaviour of such domes is of great concern because gravitational slumping of the flow front and explosive release of volatiles from the interior often initiates destructive pyroclastic flows. Extrusions of fresh magma onto the steep dome surface can also mix with rain or ice to form mudflows.

Previous fluid dynamics experiments with extrusions having a yield strength have been confined to the isothermal case (Hulme 1974; Blake 1990). Blake chose to use a suspension of kaolin in water which has the essential characteristics of a Bingham fluid: a finite shear stress at zero strain rate and a large apparent viscosity at larger strain rates. He found that for a slow extrusion from a small source on a horizontal plane (under air) the spreading was controlled entirely by the yield strength. The shape of the dome at any time was in a static balance between gravity and yield strength, and it remained axisymmetric apart from sets of conjugate spiral fracture lines faintly visible on its surface.

We report experimental results obtained using a similar slurry, but this time of kaolin in wax injected above its freezing point onto a horizontal plane beneath water, with the water at a temperature below the freezing point of the slurry. The study is primarily experimental since this is the first study of these complex and poorly understood flows. It is not clear how further theoretical analyses of the mechanisms involved can be achieved and the flows will also provide a significant challenge to future computational modelling. Observations of the flow morphology and measurements of dome height and width are compared with the previous results for

solidifying extrusions of viscous wax, isothermal extrusions of kaolin/water slurry and predictions of scaling theories. Finally, we compare the solidifying laboratory flows with aspects of several lava domes.

2. Experiments

In order to investigate the most fundamental aspects of extrusions having both a yield strength and solidification we concentrate on the case of a fluid having an approximately Bingham rheology extruded from a small source onto a horizontal plane. A mixture of a polyethylene glycol wax (PEG 600) with kaolin powder in fixed proportions (3:2) by weight was selected after measuring the viscosity and yield strength of various mixtures and testing extrusions beneath both air and water. Heat loss from the surface of the dome sufficient to cause varying amounts of solidification was achieved by injecting the working fluid beneath cold fresh water.

2.1. *Apparatus*

All runs were carried out in a box 30 cm square (figure 1). The PEG/kaolin slurry was thoroughly stirred at room temperature (21 °C to 22 °C) and placed in a large acrylic cylinder 70 cm long and 9.7 cm in diameter, having a transparent and rigid wall. During filling the cylinder was agitated to allow small bubbles of entrained air to escape. The cylinder was connected from one end through a short 2 cm diameter thick-walled hose to a heat exchanger plugged directly into the base of the tank. The other end was connected via a small pipe and a positive-displacement peristaltic pump to a water reservoir. The water and slurry in the cylinder were separated by a free piston that sealed and slid on dual O-rings. Ejection of the slurry was controlled by pumping water into the cylinder behind the piston. Motion of the piston then forced the slurry out of the cylinder, through the heat exchanger and onto the floor of the tank at the prescribed rate. Only a small air bubble ($< 5\ \mathrm{cm}^3$) was allowed in the water space behind the piston: this served to smooth the small pulsations of the pump while minimizing the compressibility of the system and giving a constant effusion rate. The heat exchanger, designed only to adjust the slurry temperature through 1 °C or less in order to remove room temperature fluctuations, consisted of four narrow channels (0.6 cm wide $\times$ 10 cm long) through which the slurry was forced before it rejoined into one pathway and entered the tank. These were surrounded by a water jacket connected to a bath held at 20.6 °C. This heat exchanger was included only to reduce any effects of small changes in room and reservoir temperatures. The injection hole in the base of the tank had a diameter 0.6 cm (smaller than that used by Blake 1990). Before and after a run, the injection hole was plugged from above in order to prevent contact between slurry and cold water.

In all 21 experiments the floor of the tank was horizontal. In most runs the floor was smooth acrylic. However, in five runs a sheet of acrylic scored with two orthogonal sets of parallel grooves (4 mm centres and 2 mm deep $\times$ 2 mm wide) was inserted as the floor of the tank. This provided a rough base and a test of the role of basal sliding.

Before each run slurry was forced through the hose and heat jacket to remove air pockets from the system. To begin each run, water at the desired temperature (between 4 °C and 20 °C) was placed in the tank to a depth of approximately 15 cm. Video records of both top and side views of the tank were started and the water temperature was checked. Simultaneously, the plug was removed and the pump was turned on. We estimated that the effusion rate took less than 3 s to reach the preset value. The video top view was recorded in time-lapse in order to greatly reduce the storage of

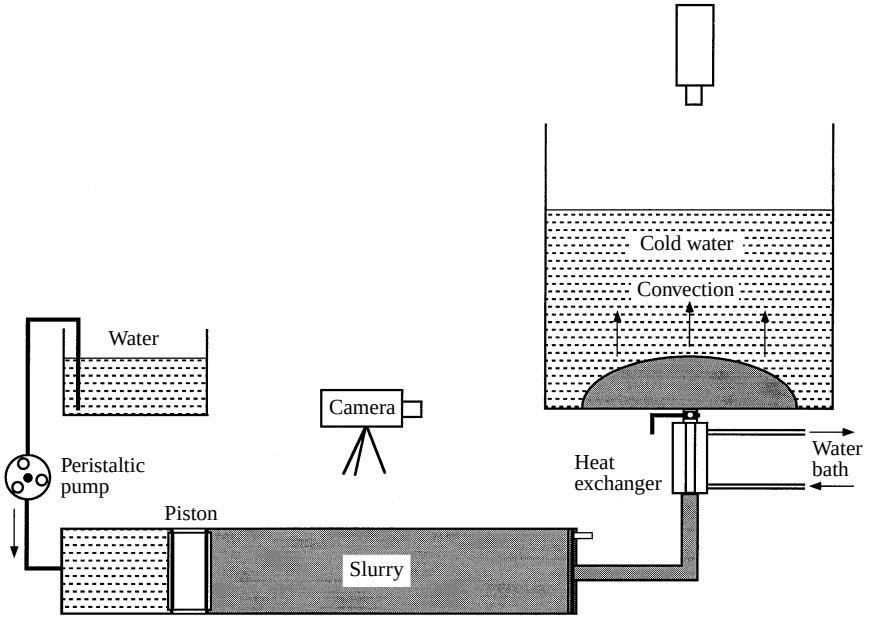

FIGURE 1. Schematic representation of the apparatus used to produce extrusions of slurry at a constant flow rate and at a constant temperature onto the base of a tank beneath cold water.

unnecessary data and facilitate more rapid selection of digitized frames. Re-play of the time-lapse record (speeding up the flow by a factor ranging from 16 to 72) was also a very useful aid, since it revealed aspects of the motion which could not be recognized when watching the experiment in real time. In addition to the video records still photographs were taken with a fixed camera above the tank and with a hand-held camera from the side or at an angle to the horizontal.

Each run was continued until either the flow reached the sidewalls of the tank or a desired volume of slurry had been ejected. Run durations ranged from 10 to 30 minutes, depending on the flow rate. Displacement of the free piston was monitored in order to determine the effusion rate Q. In most runs Q was fixed throughout the duration of the extrusion. However, in two runs the effusion rate was designed to decrease and we aimed to approximate the power laws $Q \sim t^{-0.2}$ and $t^{-0.4}$. In these cases the calibrated peristaltic pump setting was decreased in many pre-programmed steps. The accumulated volume discharge V actually achieved was again checked by measuring the piston displacement at regular time intervals: it increased as $V \sim St^{\alpha}$, where S is a constant and we achieved $\alpha = 0.80$ and 0.65.

Measurements of dome radius and height were later taken from the video records by capturing appropriate frames on a computer. Domes with significant cooling were not axisymmetric and, therefore, an average radius was calculated. Domes with rapid cooling and slow flow rate were also irregular in height. We measured the height over the vent, and this was in most cases the greatest height.

The experiments with slurry followed trial experiments with partially solidified 'cloudy' PEG. Those trials produced interesting results, with spiralling extrusive features not seen in the previous experiments with injection of liquid wax. However, they were not continued because the properties of the non-equilibrium solid/liquid suspension could not be reliably reproduced.

Property	PEG 600 (21 °C)	Slurry (21 °C)	Overlying water (4–21 °C)
Density ρ (kg m^{-3})	1.126×10^3	1.45×10^3	(A 1)
Specific heat c_p (J kg^{-1} K^{-1})	2.49×10^3	1.78×10^3	4.18×10^3
Thermal diffusivity κ (m^2 s^{-1})	0.86×10^{-7}	1.44×10^{-7}	1.3×10^{-7}
Thermal expansivity α (K^{-1})	—	—	(A 1)
Shear strength σ_0 (Pa)	0	84	—
Viscosity η (Pa s^{-1})	0.18	0.78	(A 2) $\times$ (A 1)
Kinematic viscosity ν (m^2 s^{-1})	1.6×10^{-4}	5.38×10^{-4}	(A 2)
Solidification temperature T_s (°C)	19.4	17	—

TABLE 1. Properties of polyethylene glycol (PEG, grade 600, manufactured by Dow Corning) and the 40 % by weight suspension of kaolin in PEG at 21 °C, along with relevant properties of the overlying fresh water in the tank. The viscosity given for slurry is the apparent viscosity η^* at large strain rates. Measurements and calculations of these quantities are discussed in the Appendix.

2.2. *Material properties*

The previous modelling of lava flows with solidifying wax (Fink & Griffiths 1990, 1992) made use of the convenient properties of PEG 600 (table 1). This grade of polyethylene glycol has a solidification temperature close to room temperature (18–20 °C, depending on batch and trace water content), a density greater than water (but which can be matched by the density of an aqueous salt or sugar solution), and a viscosity ($\sim 1.6 \times 10^{-4}$ m^2 s^{-1}) which is sufficiently high to give small Reynolds numbers for the flows. The same grade of PEG was used for the present slurry experiments, primarily because of its solidification temperature.

It is useful that the wax viscosity varies only by a factor of less than two with temperature, otherwise there could be difficulty in separating the effects of solidification from those of increased viscosity in the cooled surface layer. We wish to concentrate on the role of solidification because it is clear that the surfaces of lava flows solidify and fracture, and that yield strength is the cause of at least the eventual halting of the advance of the flow front. In contrast, the case of a strongly temperature-dependent purely viscous flow cooled from its surface (Stasiuk *et al.* 1993) does not show the variety of qualitatively different flow behaviours seen in the experiments with solidifying flows (Fink & Griffiths 1990, 1992) and in real lava flows (Griffiths & Fink 1992*a*, *b*, 1993).

The proportion of wax and kaolin in the slurry for our experiments was chosen so as to give a yield strength that supported a dome 2–3 cm high in static balance under air, when approximately 20 cm in diameter. This height is sufficient to allow convenient measurements. Isothermal domes formed under water were then of a convenient height also (3–4 cm). Most importantly, the yield stress was sufficiently large to ensure that the flows were dominated by the strength rather than by viscous stresses. We settled on the mixture 2.000 kaolin: 3.000 PEG by weight.

Material properties of both the slurry and PEG are summarized in table 1 and discussed further in the Appendix. Three estimates of the slurry's shear strength were obtained: one from a rotary viscometer and the others from the shape of axisymmetric isothermal domes formed under air and water. The viscometer measurements give a representative slope η^* of the stress–strain rate curve at large strain rates and could be extrapolated to find a shear stress σ_0 at zero strain rate (see figure 7). Thus we have the coefficients of the idealized Bingham relation $\sigma = \sigma_0 + \eta^* \dot{\epsilon}$, where $\dot{\epsilon}$ is the strain rate. However, as with Blake's (1990) aqueous suspension of kaolin, the viscometer

measurements are all at strain rates much larger than those typical of the experimental flows and the $\sigma(\dot{\epsilon})$ curve is nonlinear at small strain rates. Hence the extrapolation to $\dot{\epsilon} = 0$ does not demonstrate the existence of a finite yield strength and, in any case, provides an over-estimate of the actual value of σ_0. The nonlinearity could in fact be a shear-thinning behaviour which causes the stress to vanish at zero strain rate (Kerr & Lister 1991). On the other hand, our domes under both air and water were clearly in a static balance for periods of hours after the supply of slurry was turned off. We therefore conclude that the slurry had a shearing strength, and we prefer estimates of the strength obtained directly from control experiments with extrusion but no cooling.

In the control experiments, the slurry was extruded into water at the same temperature or into air using the apparatus described above and the height and radius of the domes measured as functions of time. We then constructed plots of height H versus radius R as they evolved for each dome (similar to the plots in figure 5*c* to be discussed later) and found the power-law curves of best fit. According to Nye's (1952) approximate analytical solution the shape $h(r)$ of an axisymmetric dome of uniform material in a static balance is given by

$$h^2 = 2h_0(R-r), \tag{1a}$$

which gives the central height

$$H = C(h_0 R)^{1/2}, \tag{1b}$$

where $C = \sqrt{2}$ and $h_0 = \sigma_0/g\Delta\rho$ (σ_0 is the yield stress, g the acceleration due to gravity and $\Delta\rho$ the density difference driving the spreading). Blake's data for flows under air confirmed the square-root relation in (1*b*) for both growing and stationary domes and gave an empirical value for the constant $C = 1.76$. We note that (1) is not expected to hold precisely at the origin due to the effects of relatively rapid flow (possibly controlled by viscous stresses rather than yield strength) out of a small source, nor at the flow front where the surface will be vertical or over-steepened. For a constant rate of supply of material at the origin, the radius and height of a Bingham dome were predicted to increase with time according to

$$R \sim 0.65(g\Delta\rho/\sigma_0)^{1/5}(Qt)^{2/5}, \quad H \sim 1.4(g\Delta\rho/\sigma_0)^{-2/5}(Qt)^{1/5}, \tag{1c}$$

respectively.

Our data for slurry domes under air are again consistent with the solution (1*b*) (the empirical exponent is actually 0.45 ± 0.05). Hence we assume that (1*b*) and Blake's empirical value of C apply, and estimate the yield strength $\sigma_0 = g\Delta\rho/C^2(H^2/R)$. This approach gives $\sigma_0 = 84\,\mathrm{Pa}\,(\pm 20\,\%)$. Values of σ_0 evaluated from $R(t)$ involve larger uncertainties resulting from the choice of a time origin when fitting the power law (1*c*) and from their dependence on the square of the effusion rate Q.

When the same slurry was extruded under water the dome showed a significantly different behaviour. In this case the dome height increased as $H \sim R^{0.60 \pm 0.02}$ in place of the square-root relation in (1*b*). Furthermore, if we attempt to fit the square-root relation to the data, using Blake's value for C, we obtain the smaller apparent strength $\sigma_0 = 26\,\mathrm{Pa}$. In other words, the dome under water was *lower* than expected on the basis of the behaviour of the slurry under air. We attribute these differences to reduction of the coefficient of sliding friction of the wax on the smooth tank floor due to wetting by water, and to fracturing of the dome surface which occurs under water in the region of maximum strain rate above the vent. This fracturing penetrates several millimetres into the slurry and produces a granular texture on the surface, while decreasing the effective depth of the dome that can support a given stress. Both the reduction in basal friction and the surface fracturing could cause the domes to be lower (even though the maximum height increased as a power law of dome radius R with a larger exponent).

In the experiments under air fracturing at the surface is prevented by surface tension. This maintains a smooth surface. However, surface tension is not relevant to lava flows. (The action of surface tension on the curvature of the surface of the laboratory domes under air can also inhibit spreading and increase dome height. However this effect is small, leading to an over-estimate of σ_0 by no more than 3%). We therefore take the yield stress found from domes *under air* as the best estimate of the actual strength of the slurry. Differences in the flow behaviour, such as sliding or surface fracturing, between air and water ambients are real aspects of the flow. We will also need to compare the solidifying flows under water with the isothermal flow under water.

It will be seen that a crucial factor in the behaviour of cooling domes is the rate of solidification of the dome surface. Hence, it is necessary to evaluate the heat loss from the surface due to high-Rayleigh-number thermal convection. For this we require values for the density, expansion coefficient, specific heat and viscosity of the overlying cold water. These are listed in table 1 and discussed in the Appendix.

3. Governing parameters

The complex behaviour of cooled Bingham extrusions will be presented as a spectrum which begins with axisymmetric isothermal Bingham flows. Similarity solutions for isothermal Bingham flows are given by Blake (1990), and further discussed by Griffiths & Fink (1993). They show that these flows pass from an initial regime in which motion is controlled by non-hydrostatic pressure forces and Newtonian viscous stresses to one controlled by the balance between gravitational (buoyancy) force and the yield stress. For a constant effusion rate Q the transition from non-hydrostatic to buoyancy-driven flow occurs at a time $(\eta/g\Delta\rho)^{3/4}\,Q^{-1/4}$ (Griffiths & Fink 1993) and the transition from flow controlled by basal viscous stress to one controlled by yield strength occurs at a time $t^* \sim (g^3\Delta\rho^3\eta^5Q)^{1/4}/\sigma_0^2$ (Blake 1990). Under the conditions used in our experiments these transitions are predicted to occur at times less than 0.02 s and 10^{-3} s, respectively. In effect, the extrusions are expected to have been in the buoyancy-driven and plastic regime at all times. As with extremely viscous gravity currents, the subsequent behaviour of the isothermal Bingham flows is independent of all dimensionless parameters.

For the isothermal case we have the time scale $t_A = h_0/U$ for the fluid elements to travel the distance h_0 from the source. Using the depth scale $h_0 = \sigma_0/g\Delta\rho$ and the velocity scale $U = Q/h_0^2 = Q(g\Delta\rho/\sigma_0)^2$ the advection time becomes

$$t_A = (\sigma_0/g\Delta\rho)^3\,Q^{-1}. \tag{2}$$

For the cooling and solidifying flows, the independent variables are the eruption rate Q, vent lava temperature T_l, ambient water temperature T_a, gravitational acceleration g, density difference $\Delta\rho$, and a range of material properties of the slurry and water. The surface heat flux and the rate of solidification are determined by the temperatures and fluid properties, while the depth of penetration of cooling is also a function of eruption rate. Following Fink & Griffiths (1990) we define the dimensionless temperature difference Θ_s through which the lava surface must cool before solid begins to form,

$$\Theta_s = (T_s - T_a)/\Delta T, \tag{3}$$

where $\Delta T = T_l - T_a$. The ratio of flow speed to diffusion speed can be expressed as the Péclet number $\mathrm{Pe_B}$ for a Bingham flow,

$$Pe_B = Uh_0/\kappa = (g\Delta\rho/\sigma_0)\,Q/\kappa. \tag{4}$$

The thickness of the thermal boundary layer relative to the depth scale h_0 is proportional to $Pe_B^{-1/2}$ and the whole depth of the flow near the flow front is cooled after the front has propagated a distance of order $h_0 Pe_B$. We are concerned only with flows having $Pe_B \gg 1$. However, the thermal boundary layer thickness is not the quantity of primary interest, since solidification (or any other rheological changes) will be confined to a surface layer much thinner than the thermal boundary layer.

The rate of solidification is characterized by the time t_s taken for the surface temperature to fall from T_l to its solidification temperature T_s after exposure to the overlying cold water. This time can be found by matching conductive heat flow in the dome material to a surface heat flux provided by natural convection in the water (or by radiation from lava flows under air, Griffiths & Fink 1992*a*). We assume that the rate of heat loss from the dome surface is determined entirely by turbulent thermal convection and we neglect any effect of compositional convection, although this is present in the experiments in the form of a thin dense boundary layer of water, wax and kaolin. This very thin dense layer can be seen at large times in those runs having very low effusion rates. However, owing to its stability, the compositionally driven flow is inefficient at carrying heat away from the slurry. It flows slowly down the sloping surface of the domes onto the surrounding tank floor, carrying the kaolin powder with it and eventually building up a cloudy stratified layer around the base of the dome. In contrast, thermal convection carries heat through the depth of the water and is strongest when the ambient water is coldest.

Summarizing the analysis for the surface (or contact) temperature T_c (Fink & Griffiths 1990; Griffiths & Fink 1992*a*), the surface solidification time t_s is found from the integral equation (Carslaw & Jaeger 1959, p. 76; Huppert & Sparks 1988)

$$\theta_c = 1 - \frac{1}{\rho c(\kappa\pi)^{1/2}\Delta T}\int_0^t \frac{F(\zeta)}{(t-\zeta)^{1/2}\,\mathrm{d}\zeta}, \tag{5}$$

where $\theta_c = (T_c - T_a)/\Delta T$, $T_c(t)$ is the time-dependent temperature of the contact surface, κ is thermal diffusivity and $F(t)$ is the time-dependent surface heat flux. In the experiments this flux is due to turbulent convection and is parameterized as

$$F = 0.1\rho_a c_a (g\alpha_a \kappa_a^2/\nu_a)^{1/3}(\Delta T\theta_c)^{4/3}, \tag{6}$$

where ν is kinematic viscosity and subscript a denotes ambient. In applications to lava domes (6) must be replaced by an expression for the heat loss due to both convection and radiation. The solution $t = t_s$ at $\theta_c = \Theta_s$ to (5), (6) is found numerically.†

Having the two independent time scales, t_s and t_A, we form the ratio of solidification to advection times

$$\Psi_B = t_s/t_A = (g\Delta\rho/\sigma_0)^3 Q t_s. \tag{7}$$

This we expect to serve as the primary parameter describing the effects of cooling. Large values of Ψ_B imply that solidification occurs slowly or that the eruption rate is large, whereas rapidly chilled or very slow eruptions give small values of Ψ_B. This parameter, while not strictly describing the rate of thickening of the solid crust, captures much of the roles of cooling and eruption rate because crust thickness increases more rapidly if the onset of solidification is faster, and for greater effusion rates the fluid moves farther from the vent before crust develops.

† For convenience in evaluating t_s for each experiment the solution can be written as $t_s = \lambda\tau_s(\Theta_s)$, where λ is defined in (8), and the numerical solution for the dimensionless quantity τ_s (Fink & Griffiths 1990) was fitted very precisely (for $\Theta_s > 0.4$) by the explicit polynomial expression: $\tau_s = \exp^{-1}[8.8694 + 40.443\ln\Theta_s + 135.89(\ln\Theta_s)^2 + 294.24(\ln\Theta_s)^3 + 364(\ln\Theta_s)^4 + 236.08(\ln\Theta_s)^5 + 62.111(\ln\Theta_s)^6]$.

Exp. no.	T_a (°C)	Q_0 ($m^3 s^{-1}$) ($\times 10^6$)	$\Delta\rho$ (kg m^{-3})	Comments	Regime	λ (s)	Pe_B	Θ_s	τ_s	t_s (s)	Π_B	Ψ_B
95-13	21.2	2.4	1450	Under air	A	0	1434	0	Infinite	Infinite	—	—
95-14	20.0	2.4	450	Isothermal	A	148.8	447	0	Infinite	Infinite	7.0	Infinite
95-15	20.4	1.1	1450	Under air	A	0	1317	0	Infinite	Infinite	—	—
95-16	5.5	1.1	450	—	L (S)	52.8	411	0.799	0.017	0.87	8.6	0.14
95-17	20.0	1.1	1450	Under air	A	0	1291	0	Infinite	Infinite	—	—
95-18	11.0	1.1	450	—	L	53.0	392	0.625	0.096	5.07	8.2	0.79
95-19	15.1	1.1	450	—	P	64.5	402	0.345	1.045	67.37	10.3	10.76
95-20	20.2	1.1	450	Isothermal	A	308.3	401	0	Infinite	Infinite	49.3	Infinite
95-21	5.2	3.2	450	—	L	50.7	1172	0.766	0.024	1.23	23.5	0.57
95-22	11.0	3.2	450	—	P	53.0	1149	0.625	0.096	5.07	24.1	2.31
95-23	14.8	3.2	450	—	A	62.5	1169	0.379	0.811	50.74	29.0	23.55
95-24	5.5	4.9	450	—	P (L)	51.1	1793	0.762	0.026	1.31	36.2	0.93
95-25	5.1	0.6	450	—	S	50.0	218	0.753	0.028	1.40	4.3	0.12
95-26	5.2	0.6	450	—	S	50.7	226	0.766	0.024	1.23	4.5	0.11
95-27	4.7	0.3	450	—	S	49.5	122	0.759	0.026	1.30	2.4	0.06
95-28	4.7	1.2	450	Episodic	L	49.5	419	0.759	0.026	1.30	8.2	0.22
95-29	4.9	1.2	450	—	L	49.7	449	0.756	0.027	1.35	8.8	0.24
95-30	4.8	1.1	450	$\alpha = 0.80$	L (S)	49.6	382	0.758	0.027	1.33	7.5	0.20
95-31	4.7	1.1	450	$\alpha = 0.65$	L	49.5	411	0.759	0.026	1.30	8.0	0.21
95-32	5.6	1.2	450	Rough base	L	50.6	437	0.745	0.031	1.55	8.7	0.27
95-33	5.9	1.2	450	Rough base	L	50.8	433	0.735	0.034	1.72	8.7	0.29
95-34	10.2	3.2	450	Rough base	P	51.0	1169	0.642	0.082	4.21	23.6	1.95
95-35	15.0	3.2	450	Rough base	A	62.3	1174	0.345	1.048	65.31	29.0	30.43
95-36	10.1	2.2	450	Rough base	P	50.5	812	0.639	0.084	4.26	16.2	1.37

TABLE 2. Parameter values and flow regime classifications for each experiment. The actual time scales for cooling of the slurry surface to the ambient water temperature and for the onset of solidification are included. The morphologies are classified in column 6 as 'axisymmetric' (A), 'platy' (P), 'lobate' (L) and 'spiny' (S)

As an additional aid to the understanding of the processes influencing dome growth, Ψ_B can be separated into two independent dimensionless parameters. To this end we define a third time scale λ, over which the contact temperature decreases from the vent temperature and approaches the ambient water temperature. Using the heat flux (6) it can be shown (Fink & Griffiths 1990) that

$$\lambda = 100\pi(\rho c/\rho_a c_a)^2 (\nu_a/g\alpha_a \Delta T)^{2/3} \kappa_a^{-4/3} \kappa. \tag{8}$$

Thus we can write Ψ_B as the product

$$\Psi_B = \Pi_B \tau_s, \tag{9a}$$

where $\tau_s = t_s/\lambda$ and $\Pi_B = \lambda/t_A$. On substituting from (2) the latter is simply

$$\Pi_B = (g\Delta\rho/\sigma_0)^3 Q\lambda. \tag{9b}$$

The ratio τ_s is a function only of Θ_s. The second ratio Π_B is independent of Θ_s and, like the Péclet number Pe_B, is proportional to the effusion rate. However, unlike the Péclet number, Π_B relates to the rate of cooling only at the contact surface and not to the extent of heat conduction into the flow interior. Thus Π_B and τ_s serve as two independent parameters which can be adjusted separately in experiments covering a range of conditions. The values of the dimensionless parameters for our experiments are given in table 2.

By way of contrast we recall that the corresponding form of the depth scale h_0 for the case of extrusions of viscous fluid from a point source (where the fluid is purely viscous before cooling, although it may become plastic or brittle on solidification) is $h_v = (Q\eta/g\Delta\rho)^{1/4}$ and the parameter Ψ corresponding to Ψ_B is (Fink & Griffiths 1990)†

$$\Psi = (g\Delta\rho/\eta)^{3/4} Q^{1/4} t_s. \tag{10}$$

4. Qualitative observations – dome morphology

The shape and surface texture of the domes formed by extrusion of slurry, and the style of growth, were very clearly dependent on both the ambient water temperature and the effusion rate.

In isothermal runs, where no solidification could take place (water temperature of 20 °C, $\Theta_s = 0$, $\Psi_B = \infty$), the domes grew in an axisymmetric manner. They also had a rough surface texture (figure 2*a*). This roughness developed close to the vent, where the rate of surface divergence was greatest. After the vent flow was turned off the dome retained its shape without measurable slumping, indicating that during its growth it was in a state of static balance between buoyancy forces and the yield stress. A comparison of the dome height profile (figure 3) with that predicted by (1*a*) shows a general similarity but also reveals limitations of the theoretical solution in addition to those expected at the axis and flow front. In particular, the solution over-estimates the flow depth at mid-radius, a feature also noted by Blake (1990) for his slurry domes under air.

† We note a correction to the values previously published for Ψ resulting from an error in the magnitude used for the viscosity of water: all values of Ψ quoted or graphed in Fink & Griffiths (1990, 1992) and Griffiths & Fink (1992*a*, *b*, 1993) must be decreased by the factor $10^{2/3}$. Hence the transitions between flow regimes on a smooth tank base lie at $\Psi \approx 0.7$ ('pillows' to 'rifts and plates'), $\Psi \approx 2.5$ ('rifts' to 'folds') and $\Psi \approx 6$ ('folds' to 'levees' or no crust). For rough, non-slip bases more relevant to natural lavas the transitions occur at Ψ-values similar to those previously published for smooth bases.

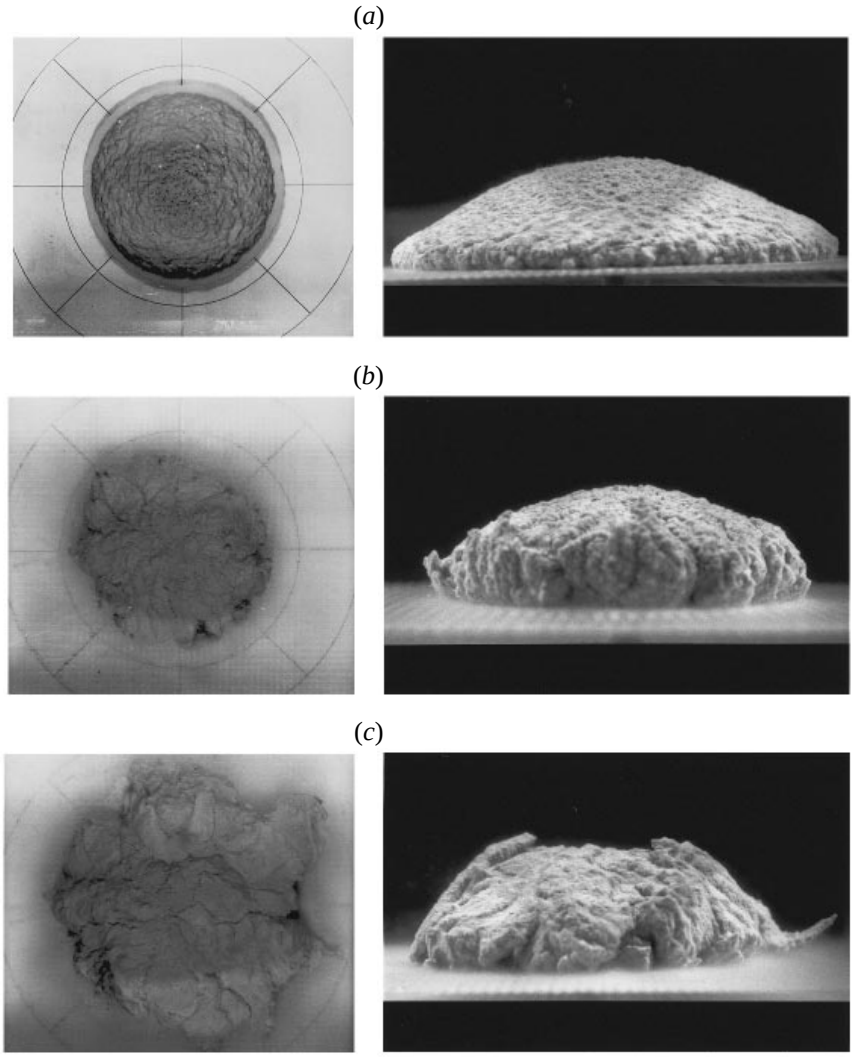

FIGURE 2(*a–c*). For caption see facing page.

For water temperatures of 10 °C and 15 °C, and large effusion rates, the domes were still largely symmetric, except for scalloping of the flow front. The irregular structure at the front developed in time as a result of the solidification of strong pieces of crust (smaller than those seen in figure 2*b*, *c*). These tended to act as levees which inhibited advance of the front, but they were also displaced by the advancing flow. They were sometimes toppled over like opening flower petals (also seen with more rapid cooling in figure 2*b*, *c*). The height profiles (figure 3) show that, while the solid at the flow front sometimes increased the flow depth near the flow front, there was little change in the overall shape of the domes. The surface texture remained rough and fragmented, and growth was entirely by inflation ('endogenous'). On the rough surface faint lines could be seen forming conjugate sets of spirals. These are the fracture surfaces previously identified in the isothermal case (Blake 1990). In some cases we also identified small folds transverse to the radial compressive stress. We refer to this style of dome growth as 'leveed' or 'axisymmetric'.

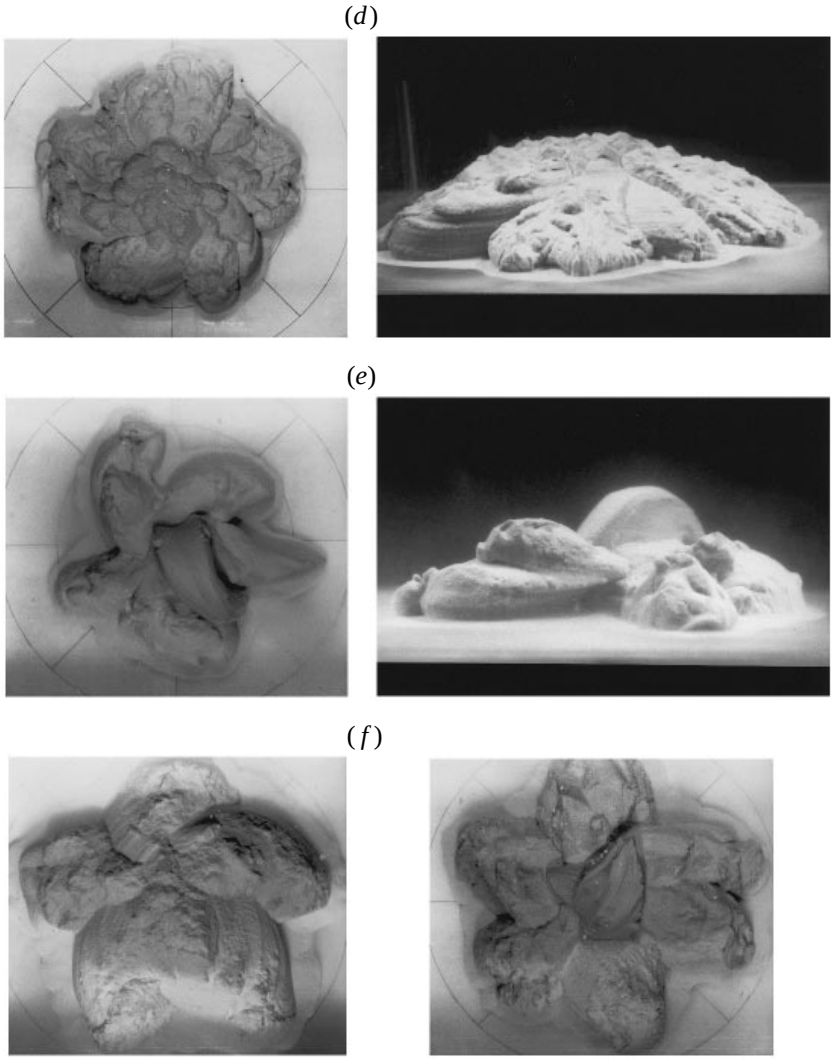

FIGURE 2. Photographs of sample experiments showing top (left) and side (right) views of (*a*) nearly adiabatic flow, $\Psi_B = 30.4$, classified as 'axisymmetric' and not significantly different from perfectly adiabatic cases (experiment no. 95-35); (*b*) and (*c*) two stages in the development of a run having a mild cooling rate, $\Psi_B = 1.37$ and classified as 'platy' (no. 95-36, though extrusive ridges were not evident in this run until times much later than shown); (*d*) moderately rapid cooling and small effusion rate, $\Psi_B = 0.57$ and classed as 'lobate' (no. 95-21); (*e*) rapid cooling and very small effusion rate, $\Psi_B = 0.11$ and classed as 'spiny' (no. 95-26); (*f*) two additional examples of 'lobate' flows illustrating the strong tendency for five initial lobes (experiments no. 95-18, $\Psi_B = 0.79$, and no. 95-31, $\Psi_B = 0.21$). The latter also illustrates the appearance of 'spines' late in the growth of lobate domes having Ψ_B not much greater than 0.12.

At small-to-moderate cooling rates and moderate effusion rates freezing of the dome surface took place within 1 or 2 cm from the centre (figure 2*b*, *c*). Between four and six rigid surface plates formed, their divergent boundaries producing a star pattern of approximately radial junctions, or spreading lines, centred on the vent (these are more readily visible in video records than in still photographs). The plates tended to enlarge as they were pushed apart. Thus the dome growth was still endogenous, although at

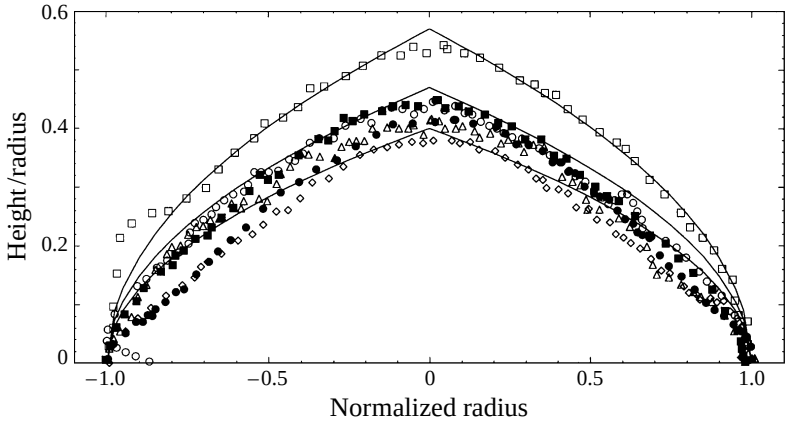

FIGURE 3. Profiles of height across the width of domes for an isothermal extrusion under water, and four domes with slow solidification. In order to facilitate comparison of different domes both the radius and height have been normalized by the radius of each dome. For comparison, Nye's (1952) solution for a static balance of uniform yield stress and buoyancy is plotted using axial heights which produce the best matches with the measurements ($H/R = 0.4, 0.47, 0.57$). Note that the height and aspect ratio of an isothermal dome is expected to decrease with time and there is no unique value for the normalized height. Two profiles are shown for experiment 95-34: the first gives a very close match to Nye's solution, whereas the later profile (like those for the other experiments) shows a relative depression in height near mid-radius. This is evident also in the isothermal case. ■, no. 95-20, $\Psi_B = \infty$; ●, no. 95-23, $\Psi_B = 23.6$; ◇, no. 95-19, $\Psi_B = 10.8$; □, no. 95-34 (120 s) and ○, no. 95-34 (480 s), $\Psi_B = 2.0$; △, no. 95-24, $\Psi_B = 0.93$.

large times the rifts tended to be replaced by solidified ridge-like extrusions. The surface was predominantly rough and sometimes formed small step-like ridges, but the later ridge extrusions were smooth. We refer to this style as 'platy'.

For colder water or small eruption rates ($\Theta_s \sim 0.75$, $\Psi_B \sim 0.3$) all of the surface was solid and the domes were asymmetric and lobate (figure 2*d*, *f*). Spiral curvature of the lobes was an obvious and dominant feature. Four to six lobes formed in the early stages of growth and developed into individual extrusions, often with only one of them actively extending at any given time. The style of dome growth under these conditions tended to change with time, from simple inflation for a short initial period to extrusion of lobes through most of the experiment. Near the end of these runs (especially for the most rapid cooling or slowest extrusion rates) erect angular extrusions, which we call 'spines', appeared close to the vent. Sometimes a single vertical protrusion formed. The flow involved both inflation and extrusion. The extrusive mode we refer to as 'exogenous', not because molten slurry was ejected onto the surface to freeze, but because growth involved ejection of individual, partly solidified extrusions. The surface texture was intermediate between that in runs having smaller and larger Ψ_B: there was some small-scale roughness but the surface was more bumpy than fragmented. We refer to this flow regime as 'lobate'.

At still lower water temperatures and small effusion rates the style of growth was purely extrusive, or 'exogenous' (figure 2*e*). Only one extrusion grew at any time, first building up a dome having four to six extrusions in immediate contact with the base and later adding extrusions ('spines') which came out on the top of the dome in the vicinity of the vent. Under these conditions there was little or no inflation of each lobe or of the dome as a whole, and growth was only by extrusion. The surface texture was dominated by very smooth areas that showed only flow-wise grooves formed by extrusion of the material. We refer to this regime as 'spiny'.

At the most extreme cooling and slowest effusion rates the flow in the 'spiny' regime became noodle-like and reminiscent of extruding toothpaste. The solid crust thickened so quickly that an extrusion could support its own weight until it had grown longer than its width, after which the extrusions broke and fell over onto the base of the tank or onto the top of the dome, where they then became locked. The vent flow was diverted to begin another extrusion. The consequent dome was highly irregular in form.

Under conditions intermediate between those giving either very rapid solidification on the one hand or little solidification on the other (i.e. in the 'platy' and 'lobate' regimes) the nature of the dome growth often appeared to evolve in time. At early times the dome was relatively symmetric, regular in shape but rough in texture, and growth was by inflation. At later times the effects of solidification became more obvious and the morphology could be classified as either 'platy' or 'lobate', as described above. The initial period of inflation was shorter for smaller Ψ_B, and was not apparent at all for $\Psi_B < 0.15$. This early period of inflation possibly represents an initial regime dominated by the interior yield strength, followed by a transition to a regime in which spreading is controlled by the solidifying crust. The scaling developed in Griffiths & Fink (1993) can be used to derive the time t_c^* at which this transition is expected to occur. We find $t_c^* \sim (\sigma_0/\sigma_{0c})^{10}(g\Delta\rho/\sigma_0)^2\kappa^{-5}Q^4$, where σ_{0c} is the effective yield strength of the complex surface layer. A value of $\sigma_{0c}/\sigma_0 > 20$ would assure that $t_c^* < 100$ s in our experiments. While this strength contrast is likely to have been exceeded, we do not have a reliable measure of the surface layer strength.

In those runs which had been dominated by separating surface plates (moderate to large Ψ_B) there was also a tendency for dome growth to slowly become more extrusive at large times. In 'lobate' runs a central, almost vertical and pointed spine often appeared toward the end of the experiment. This evolution may be due to the decrease in strain rates that follows the radial expansion of the flow front and is therefore consistent with the effusion rate dependence of the behaviour. However, the changes in flow style are too slow and subtle for us to conclude that there is a change in the morphological regime with time for those runs having constant effusion rates.

The range of qualitative behaviour of the flows suggests a classification based on the dominant morphology and style of growth. Thus we have classified each experiment into one of the four categories described above: 'axisymmetric', 'platy', 'lobate', and 'spiny'. The results are summarized in figure 4 in terms of the parameter pairs (Pe_B, Θ_s) and (Π_B, τ_s). The pre-defined styles of flow cluster in groups in Péclet number and Θ_s, with both temperature and effusion rate influencing the behaviour of the flow. However, we believe that Π_B is more relevant to the character of the flow than is the Péclet number.

In figure 4(*b*) we also show the contours of Ψ_B at values which best separate the regimes. Uncertainties in Π_B and Ψ_B are of the order of 60% as a result of the uncertainty in the yield stress, but this is systematic and does not influence the relative values from run to run. The results show that growth is dominated by extruded spines with smooth grooved surfaces for $\Psi_B < 0.12 \pm 0.02$, by extrusion of large and generally curved lobes with relatively rough surfaces for $0.12 < \Psi_B < 0.9 \pm 0.3$, by separation of solid plates with rough, fragmented surface texture for $0.9 < \Psi_B < 15 \pm 5$, and by purely endogenous inflation of circular domes for $\Psi_B > 15$. Results from five runs on a very rough floor are included in figure 4, but are not distinguished because they show no variation from the runs on a smooth floor. Even lobes having solid crust over 1 cm thick at the flow front slid over the rough floor, which left deep grooves in the base of the flow front. At larger Ψ_B the rough base caused solid levees to be overturned rather

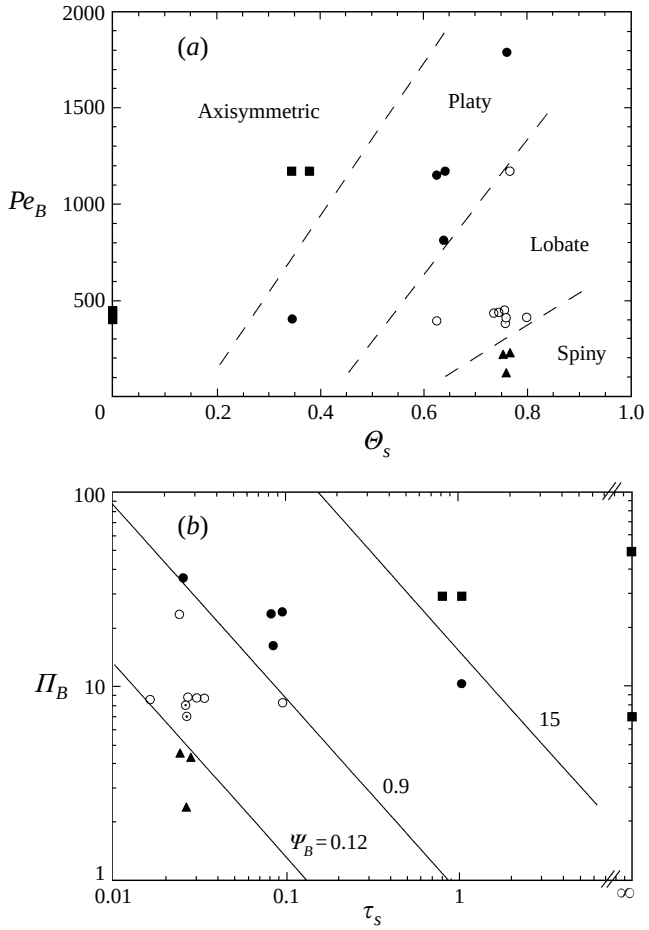

FIGURE 4. The flow regimes and their dependence on (*a*) Pe_B and Θ_s, and (*b*) Π_B and τ_s. In (*b*) the lines of constant Ψ_B are shown for values which best separate the classifications. Each experiment is classified according to the style of flow: ■, axisymmetric with no solid or only solid levees at the flow front (referred to as 'axisymmetric'); ●, solid plates over most of the surface and eventual extrusion of ridges from the divergent plate boundaries (referred to as 'platy'); ○, extruding lobes; ⊙, again extruding lobes, for two runs with decreasing effusion rate, classified as 'lobate', ▲, extruding spines in a run classified as 'spiny'.

than pushed along by the advancing flow. The results from the two experiments with decreasing effusion rates are identified in figure 4 at parameter values based on the average effusion rates, and the morphologies are consistent with those given by constant effusion rates.

The data are consistent with the hypothesis that Ψ_B is the primary parameter determining the character of a dome, at least for a given material. A similar conclusion concerning the role of the corresponding parameter Ψ (equation (10)) was reached in the previous studies of solidifying wax. However, the morphologic regimes observed in the present Bingham extrusions are quite different from those found with viscous wax. We conclude that the difference is due to the yield strength of the slurry before it is cooled by the environment.

On draining the water from the tank immediately after a run was finished we found that the domes collapsed to varying extents due to the increased buoyancy force. The

extent of collapse was greater for runs having smaller amounts of solid crust. However, all of the domes remained otherwise undisturbed and it was possible to dissect them and observe the thickness of crust. This ranged from less than 1 mm (for the larger effusion rates and overlying water at 15 °C) to over 10 mm (for small flow rates and water at 5 °C). The thickness of solid increased from a minimum near the vent to a maximum at the flow front. In 'lobate' cases the crust thickness also increased with the age of the lobe.

5. Dome height and radius

In order to investigate the dynamics of growth of the laboratory domes we compared the evolution of average radius and height for domes across the range of experimental conditions. Although the results are not particularly revealing and do not focus on the flow structure caused by cooling, we present them here for completeness.

Plots of the average dome radius R and height H (figure 5) reveal that the growth in all runs is very well described by simple power laws. This is evidence that the dynamics governing the overall growth of each dome was constant throughout most of the duration of an experiment (i.e. dome growth was close to self-similar). The only irregularity occurred in runs with rapid solidification and small effusion rates (small Ψ_B), where the central height did not increase uniformly in time. This was a result of the extrusion of individual lobes, with some lobes rising and then collapsing onto the base and later ones protruding as vertical spines.

The exponents of the power laws of best fit, summarized in figure 6 as functions of Ψ_B, potentially discriminate between the various possible dynamical force balances. For experiments with large values of Ψ_B (> 0.9) the exponents are independent of the parameters and apparently are not influenced by cooling. The average exponents from six runs having surface cooling but $\Psi_B > 0.9$ give $R \sim t^{0.42\pm0.02}$, $H \sim t^{0.25\pm0.01}$, and $H \sim R^{0.60\pm0.01}$. For rapid solidification, on the other hand, where growth was by extrusive lobes or spines ($\Psi_B < 0.9$), the results are significantly more scattered, probably as a result of the timing and position of the growth of spines. Under these conditions the dome radius tended to grow more slowly and the height more rapidly, than at large Ψ_B: averaging results from five experiments having $\Psi_B < 0.2$ and constant effusion rate we find $R \sim t^{0.37\pm0.07}$, $H \sim t^{0.288\pm0.024}$ and $H \sim R^{0.79\pm0.19}$.

Under all conditions the dome height increased significantly more rapidly (with both time and radius) than was predicted and measured for uniform adiabatic Bingham domes under air (equation (1*b*, *c*); Blake 1990). The results at $\Psi_B > 0.9$ appear to be more consistent with the predictions for a solidifying dome in which the yield strength in a thin surface crust is the dominant resistance to spreading (scaling analysis predicts $R \sim t^{3/8}, H \sim t^{1/4}, H \sim R^{2/3}$; Griffiths & Fink 1993). A complication, however, is that the isothermal dome formed under water shows identical behaviour to those with some cooling. Thus (while recalling that the measurements of radius and dome height have been designed to average over the strong flow asymmetries produced by solidification) we conclude that cooling and solidification do not significantly alter the overall height and average radius of domes under these conditions. On the other hand, it is clear that the results are not consistent with the predictions for viscous spreading, whether isothermal (for which the flow height is constant, Huppert *et al*. 1982) or with a cooled, more viscous surface layer (Griffiths & Fink 1993).

At $\Psi_B < 0.9$ the behaviour may be transitional from a balance between buoyancy and a plastic crust, as at larger Ψ_B, to a balance between internal pressure and crust strength in runs with very small Ψ_B, where the crust is very thick. If this is the case, the

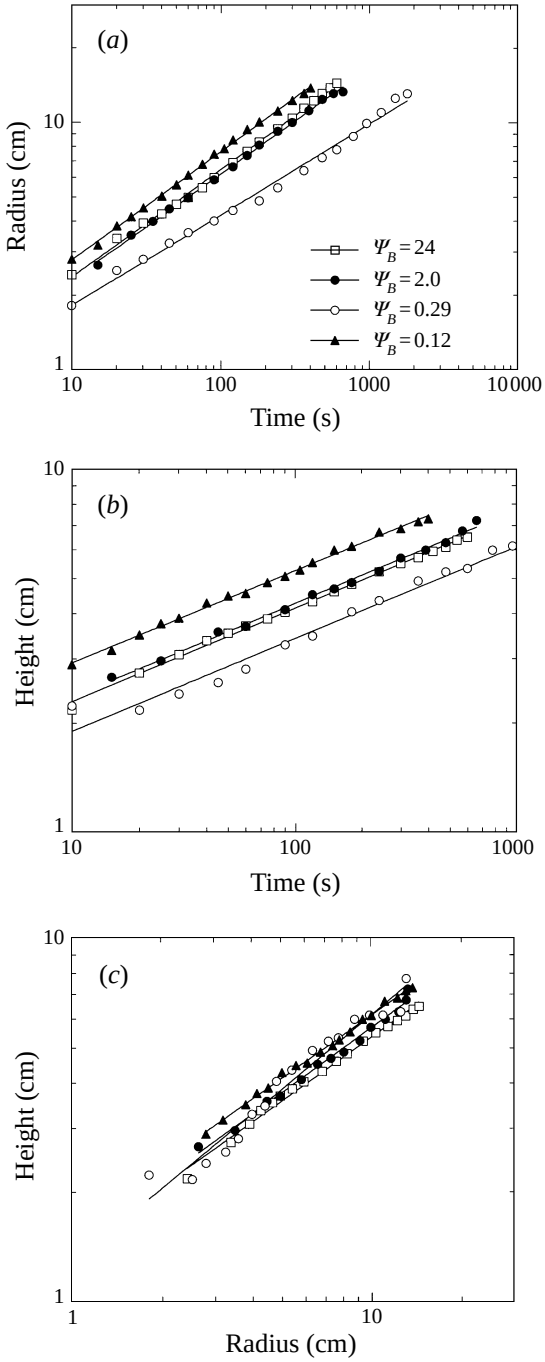

FIGURE 5. The evolution of (*a*) dome radius as a function of time, (*b*) dome height as a function of time and (*c*) dome height as a function of dome radius for sample experiments at different values of Ψ_B. Although there are kinks in the evolution of dome height at the small values of Ψ_B, in all cases the behaviour is very well described by simple power laws. (The results shown are from experiments, in order of increasing Ψ_B, nos 95-23, 95-34, 95-33 and 95-25.)

power-law exponents should trend toward $R \sim t^{1/3}$, $H \sim t^{1/3}$, and $H \sim R$, as indicated in figure 6. However, the small difference between these two limits, and the inevitable scatter for runs having individual lobes and spines, prohibit a definite conclusion.

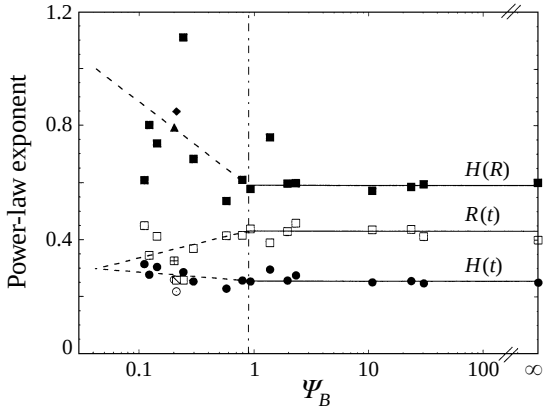

FIGURE 6. The power-law exponents for all experiments as functions of Ψ_B. Solid lines are best fits to the data at $\Psi_B > 0.9$. Dashed lines are merely indications of the trend in the data and of an expected trend toward the predicted exponents for the over-pressure-dominated regime at very small values of Ψ_B. Buoyancy appears to be the dominant driving force for $\Psi_B > 0.9$. The symbols ◆, ▲ (for $H(R)$), squares (for $R(t)$) and circles (for $H(t)$) represent results from the two runs having decreasing effusion rates.

There is also only a small difference between the behaviours predicted for isothermal Bingham domes and those predicted for domes controlled by a solidifying Bingham crust. This motivated the two experiments in which the effusion rate was decreased in time to give $Q \sim t^{\alpha-1}$, where $\alpha = 0.8$ and 0.65. The models predict that the exponent for $H(t)$ should have been shifted to smaller values by the decreasing effusion rate if the flow was viscous (in which case the height decreases with time), and to larger values if yield strength provided the dominant control. Furthermore, if the internal yield strength of the erupted fluid were dominant, the predicted height would follow $H \sim t^{\alpha/5}, H \sim R^{1/2}$ (i.e. the aspect ratio is not dependent on the evolution of effusion rate). On the other hand, if the flow were cooling controlled, we predict $H \sim t^{1/4}$ and $H \sim R^{2/(4\alpha-1)}$. The two runs having $\alpha < 1$ (identified on figure 6) gave $H(t)$ exponents of 0.26 and 0.22, which are similar to the values for $\alpha = 1$ and consistent only with cooling control and a strong crust. They also gave $H(R)$ exponents of 0.79 and 0.85, which are again consistent with only the cooling-controlled model (although they are not as large as predicted, most probably due to a transition in the dominant driving force from buoyancy to over-pressure). Thus we conclude that the heights of the slurry domes for $\Psi_B < 0.9$ were influenced by cooling and solidification.

6. Relationships to solidifying viscous extrusions

The overall behaviour of dome radius and height for the slurry experiments was much less dependent on the ambient temperature and effusion rate than was the case for extrusions of PEG wax alone. In that case the wax had no yield strength before solidification and the flow regime varied from an isothermal viscous flow at large Ψ, through a buoyancy–crust-strength balance at intermediate values of Ψ to a pressure–crust-strength balance at very small Ψ. With no solidification the height was constant in time, whereas at small Ψ it increased at a similar rate as for the slurry domes. Hence, the addition of an internal yield strength in the present experiments influences dome height when $\Psi_B > 0.9$, where cooling and solidification have relatively little effect on the dome height. The style of dome growth and deformation of the solidifying crust, on the other hand, are strongly influenced by the addition of an internal yield strength at all $\Psi_B < 15$. In particular, a regime which is characterized by

transverse folding of a thin crust on a viscous flow is not observed on the Bingham flow. Instead, the slurry shows a transition from a leveed 'axisymmetric' flow to one dominated by plates. The 'platy' regime is similar to the 'rifting' regime identified on viscous wax flows, but is different in that the plates remain relatively equal in size and the flow front remains more nearly axisymmetric. Perhaps the greatest qualitative difference resulting from internal strength occurs at small Ψ_B, where the extrusion of relatively large lobes or spines, which have a thick crust, replaces the formation of relatively small bulbous 'pillows' in viscous flows.

On the other hand, it is clear that surface cooling and the development of solid crust is entirely responsible for the variation of the Bingham extrusions from simple axisymmetric flows. Thus we need to reconcile the obvious and important role of a strong crust with the observation that the internal strength causes the major difference between viscous and Bingham extrusions at all values of Ψ_B. We suggest that the effects of the internal yield stress in flows having strong crust arise through its restriction of flow in the interior from the vent to the flow front or to other outbreak points. New lobes or spines therefore tend to extrude from weak areas in the crust close to the vent, and the flow is fed to only one large extrusion at any one time. This behaviour contrasts with the formation of many bulbous pillows and effusion from numerous opening rifts which can occur far from the vent for viscous flows. The role of the interior rheology actually becomes more significant for smaller Ψ_B because the development of thicker solid crust leaves smaller interior channels. For the same reason the interior yield strength may also lead to a greater role of over-pressure relative to buoyancy.

7. Conclusions

Our experiments with a solidifying Bingham slurry have revealed styles of flow which are very different from those previously identified in experiments with gravity currents of solidifying viscous wax. That previous analogue proved useful in providing a framework within which we could understand the various types of mafic (relatively low viscosity) lava flows. In particular, the ratio of time scales for solidification and lateral viscous flow, Ψ, was identified as a dimensionless parameter whose value delineated a number of dynamical and morphological flow regimes, both in the wax experiments and in natural lava flows. For the Bingham extrusions we again find that an equivalent parameter, Ψ_B, this time based on height and velocity scales for plastic flow, serves well to delimit a sequence of regimes distinguished by the style of dome growth, its morphology and surface texture. The qualitative style of flow is again controlled by cooling and solidification of a surface crust. However, it is the internal yield stress which causes the behaviour to be very different from that in viscous flows. Thus the experiments indicate very significant modifications to gravity-driven flows resulting from both surface solidification and addition of an internal yield strength. These results for Bingham extrusions may be more relevant to highly silicic lava domes than were the results for solidifying viscous flows.

The experimental results are consistent with many recorded aspects of highly silicic extremely viscous (andesite, dacite and rhyolite) lava domes. In the framework of the previous viscous eruption model these domes could be seen only as anomalously large 'pillows' by analogy with submarine pillow basalts at mid-ocean ridges, if growth were endogenous, or as a field of many 'pillows', if the domes were formed by extrusions onto their surfaces. However, the formation of basalt pillows is a rapid process and only a thin crust is produced during their formation. From the Bingham analogue and its parameterization we find instead that the large lava domes may be expected to take on

various growth styles depending on the value of Ψ_B. If the effusion rate is large enough and yield strength small enough (large Ψ_B), they may be almost symmetric domes which grow by inflation and are covered with thin plates of solid crust, consistent with our own field observations (October 1995) of the appearance of the active dome in the summit crater of Mount Merapi, Indonesia. Under slower effusion rates and larger yield strengths they may grow partly by inflation (endogenously) and partly by extrusion of large lobes, as was observed for the Mt St Helens lava dome in 1981–6 (Swanson & Holcomb 1990; Anderson & Fink 1990; Fink *et al.* 1990) and the Mt Unzen dacite lava dome in 1991–3 (Nakada & Fujii 1993). When the effusion rate is very small and the magma very strong the experiments reveal a greater tendency for the erupting lava to form a sequence of large lobes like those which formed on Mt Unzen, although that dome may have been influenced by its growth on a steep mountain slope. The lobate form of growth may also involve an evolution from laterally moving lobes during the earlier stages of the growth of a laboratory dome to tall vertical spines at larger times, and this progression is enhanced by a decrease in the eruption rate with time. This progression is again similar to the behaviour of the Mt Unzen eruption which, after a large decrease in the effusion rate, ended with the ejection of a tall spine. These are intriguing relationships involving eruption rate and magma yield strength which will need to be tested by evaluation of effusion rates, solidification times scales and Ψ_B for a range of lava domes, and correlation of these with the real dome morphologies. Furthermore, since volatile gas pressure is a central factor in determining the dangers posed by explosive collapses of active lava domes, and the release of volatiles from the erupting magma is likely to be more strongly inhibited by stronger and thicker surface crust, it is logical to suppose that explosive collapses may be, at least in part, related to the style of dome growth determined by magma rheology and effusion rate. Hence, observations of the style of dome growth and the resulting flow morphology have the potential to serve as one indicator of the probable hazards of a lava dome.

We thank Tony Beasley for construction of equipment and assistance with the experiments. Research was supported by NASA Grant NAGW 529 from the Planetary Geology and Geophysics Program, National Science Foundation Grant OCE 93-16831, and a Visiting Fellowship from The Australian National University.

Appendix. Material properties

PEG/kaolin slurry

The PEG wax was slightly heated and stirred to ensure it was completely molten, then a quantity of order 10 kg was weighed (to ± 0.1 g) and the kaolin powder added until the required total weight was reached. After thorough mechanical stirring the slurry was kept in an airtight bucket until loaded into the supply cylinder. Each batch was sufficient for about six runs. The solidification temperature of PEG is a strong function of water content for very small water fractions, and it was discovered that heating of PEG in an open container led to a decrease in its solidification temperature by tenths of degrees, presumably as a result of absorption of water from the room air. Care was therefore taken to prevent prolonged exposure of the slurry to air.

Some material properties of the slurry (table 1) were measured, others calculated from those of kaolin and PEG. The density was measured to $\pm 0.5\%$ at room temperature by weighing a known volume. The specific heat was calculated as the average of those for PEG and kaolinite (for which $c_p = 710$ J kg^{-1} K^{-1}, *International*

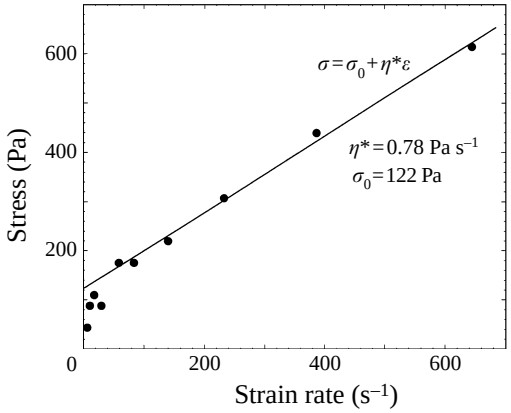

FIGURE 7. The measured stress versus strain rate for the PEG/Kaolin slurry at 20.6 °C. A linear extrapolation to zero strain rate over-estimates the actual yield stress.

Critical Tables 1928) weighted by the mass fractions. The thermal conductivity K of the slurry was estimated from the conductivities of kaolinite and PEG using the formula $K^{-1} \approx 0.6K_{wax}^{-1} + 0.4K_k^{-1}$, where $K_{wax} = 0.24$ W m^{-1} K^{-1} (Kerr 1994) and $K_k = 2.4$ W m^{-1} K^{-1} (Weast 1977; *International Critical Tables* 1928). Thus the smaller wax conductivity is dominant in producing $K \approx 0.37$ W m^{-1} K^{-1}. The thermal diffusivity is $\kappa \approx K/\rho c \approx 1.44 \times 10^{-7}$ m^2 s^{-1}.

The solidification temperature T_s of the slurry was determined by measuring the torque (and apparent viscosity) exerted by the rotary viscometer at a given strain rate, as a function of temperature at temperatures above T_s. Samples were held at the desired temperature for 30 minutes. The torque increased slowly as the temperature was decreased from 25 °C until, between 19 °C and 20 °C, it became a steep function of temperature. Small samples of the slurry at room temperature were also placed on a spatula and dipped into a water bath over a range of water temperatures from 15 °C to 20 °C. We found the approximate time required for a solid quenched layer to develop on the sample. At the lowest water temperatures this was only a few seconds, but the time versus temperature curve steepened at larger temperatures, until no apparent solid formed in two hours at 17.0 °C. The viscosity and quench time therefore provided two bounds to the solidification temperature relevant to the experiments, in which extrusions were produced over times up to 30 minutes. Thus $T_s = 17.0 \pm 0.3$ °C for the slurry, a value lower than the corresponding temperature found for the PEG alone. We note that the properties of PEG are not ideal since solidification occurs extremely slowly at higher temperatures, even at 21 °C, if the sample is stored at that temperature for one to three days. Thus we use the temperature at which a sample of slurry solidifies on the time scale of the experiments, rather than the true freezing point.

The viscometer, with coaxial cylinders in a temperature-controlled water jacket, provided data for shear stress σ as a function of strain rate $\dot{\epsilon}$ at the working temperature of 20.6 °C (figure 7). A straight line fit gave an estimate of the apparent viscosity η^* and extrapolation gave a first estimate of the shearing strength σ_0. However, the latter is expected to be significantly larger than the actual yield stress relevant to the experiments. Thus the (smaller) shearing strengths obtained from control experiments with isothermal domes, discussed in §2, are considered more reliable and appropriate.

Water

Molecular properties of the water must be known in order to evaluate the heat transport and the time scale for the dome surface to cool to the solidification temperature (see equations (6)–(8). The water density is given by a simple cubic polynomial expression in temperature (Ruddick & Shirtcliffe 1979):

$$\rho_a = \rho_0 - 2.539\times10^{-4}(T-20) + 4.968\times10^{-6}(T-20)^2 + 2.7\times10^{-8}(T-20)^3, \quad \text{(A 1)}$$

where $\rho_0 = 997.08$ kg m^3 is the density at 25 °C and T is the ambient water temperature in the tank. The thermal expansion coefficient $\alpha = \rho_a^{-1}(\partial\rho_a/\partial T)$ is found from (A 1). However, the expansion coefficient is relevant only to estimating the convective heat flux from the slurry near the vent. Hence we evaluate α at the average temperature of the ambient water and the slurry (as an approximation to the mean temperature in the thermal boundary layer driving the convection, Griffiths & Fink 1992*a*). Values of α_a vary from 1.2×10^{-4} to 2.2×10^{-4} °C^{-1} for average temperatures between 10 °C and 20 °C.

The water viscosity ν_a is a weak function of temperature. Over the range 4 °C to 20 °C it is well represented by a linear fit to published data (Weast 1977):

$$\nu_a = 1.7331\times10^{-6} - 4.6852\times10^{-8}T + 5.3363\times10^{-10}T^2, \quad \text{(A 2)}$$

where T is degrees Celsius.

REFERENCES

Anderson, S. W. & Fink, J. H. 1990 The development and distribution of surface textures at the Mount St. Helens dome. In *Lava Flows and Domes: Emplacement Mechanisms and Hazard Implications* (ed. J. H. Fink). IAVCEI Proc. in Volcanology, vol. 2, pp. 25–46.

Blake, S. 1990 Viscoplastic models of lava domes. In *Lava Flows and Domes: Emplacement Mechanisms and Hazard Implications* (ed. J. H. Fink). IAVCEI Proc. in Volcanology, vol. 2, pp. 88–128.

Carslaw, H. S. & Jaeger, J. C. 1959 *Conduction of Heat in Solids*. Oxford University Press.

Fink, J. H. & Griffiths, R. W. 1990 Radial spreading of viscous-gravity currents with solidifying crust. *J. Fluid. Mech.* **221**, 485–510.

Fink, J. H. & Griffiths, R. W. 1992 A laboratory analog study of the morphology of lava flows extruded from point and line sources. *J. Volcanol. Geotherm. Res.* **54**, 19–32.

Fink, J. H., Malin, M. C. & Anderson, S. W. 1990 Intrusive and extrusive growth of the Mount St. Helens lava dome. *Nature* **348**, 435–437, 1990.

Gregg, T. K. P. & Fink, J. H. 1995 Quantification of submarine lava-flow morphology through analog experiments. *Geology* **23**, 73–76.

Griffiths, R. W. & Fink, J. H. 1992*a* The morphology of lava flows under planetary environments: predictions from analog experiments. *J. Geophys. Res.* **97**, 19739–19748.

Griffiths, R. W. & Fink, J. H. 1992*b* Solidification and morphology of submarine lavas: a dependence on extrusion rate. *J. Geophys. Res.* **97**, 19729–19737.

Griffiths, R. W. & Fink, J. H. 1993 Effects of surface cooling on the spreading of lava flows and domes. *J. Fluid Mech.* **252**, 667–702.

Hallworth, M. A., Huppert, H. E. & Sparks, R. S. J. 1987 A laboratory simulation of basaltic lava flows. *Mod. Geol.* **11**, 93–107.

Hulme, G. 1974 The interpretation of lava flow morphology. *Geophys. J. R. Astron. Soc.* **39**, 361–383.

Huppert, H. E., Shepherd, J. B., Sigurdsson, H. & Sparks, R. S. J. 1982 On lava dome growth, with application to the 1979 lava extrusion of the Soufrière of St Vincent. *J. Volcanol. Geotherm. Res.* **14**, 199–222.

Huppert, H. E. & Sparks, R. S. J. 1988 Melting the roof of a magma chamber containing a hot, turbulently convecting fluid. *J. Fluid Mech.* **188**, 107–131.

International Critical Tables of Numerical Data 1928 *Physics*, *Chemistry and Technology*. McGraw-Hill.

Iverson, R. M. 1990 Lava domes modelled as brittle shells that enclose pressurised magma, with application to Mount St. Helens. In *Lava Flows and Domes: Emplacement Mechanisms and Hazard Implications* (ed. J. H. Fink). IAVCEI Proc. in Volcanology, vol. 2, pp. 47–69.

Kerr, R. C. 1994 Melting driven by vigorous compositional convection. *J. Fluid Mech.* **280**, 255–285.

Kerr, R. C. & Lister, J. R. 1991 The effects of shape on crystal settling and on the rheology of magmas. *J. Geology* **99**, 457–467.

McBirney, A. R. & Murase, T. 1984 Rheological properties of magmas. *Ann. Rev. Earth Planet. Sci.* **12**, 337–357.

Nakada, S. & Fujii, T. 1993 Preliminary report on the activity at Unzen Volcano (Japan) November 1990–November 1991: Dacite lava domes and pyroclastic flows. *J. Volcanol. Geotherm. Res.* **54**, 319–333.

Nye, J. F. 1952 Mechanics of glacier flow. *J. Glaciol.* **2**, 82–93.

Pinkerton, H. 1987 Factors affecting the morphology of lava flows. *Endeavour* **11**, 73–79.

Ruddick, B. R. & Shirtcliffe, T. G. L. 1979 Data for double diffusers: Physical properties of aqueous salt-sugar solutions. *Deep-Sea Res.* **26A**, 775–787.

Stasiuk, M. V., Jaupart, C. & Sparks, R. S. J. 1993 Influence of cooling on lava-flow dynamics. *Geology* **21**, 335–338.

Swanson, D. A. & Holcomb, R. T. 1990 Regularities in growth of the Mount St. Helens dacite dome, 1980–1986. In *Lava Flows and Domes: Emplacement Mechanisms and Hazard Implications* (ed. J. H. Fink). IAVCEI Proc. in Volcanology, vol. 2, pp. 1–24.

Weast, R. C. 1977 *Handbook of Chemistry and Physics*. CRC Press.